

# Determination of the local structure of a cage with an oxygen ion in $\text{Ca}_{12}\text{Al}_{14}\text{O}_{33}$

Terutoshi Sakakura,<sup>a</sup> Kiyooki Tanaka,<sup>b\*</sup> Yasuyuki Takenaka,<sup>c</sup> Satoru Matsuishi,<sup>d</sup> Hideo Hosono<sup>d</sup> and Shunji Kishimoto<sup>e</sup>

<sup>a</sup>Ceramics Research Laboratory, Nagoya Institute of Technology, Asahigaoka 10-6-29, Tajimi 507-0071, Japan, <sup>b</sup>Omohi College, Graduate School of Materials Science and Engineering, Nagoya Institute of Technology Gokiso-cho, Showa-ku 466-8555, Japan, <sup>c</sup>Hokkaido University of Education Hakodate, Hachiman-cho 1-2 Hakodate 040-8567, Japan, <sup>d</sup>Frontier Research Center Tokyo Institute of Technology, Nagatsuta-cho 4259, Midori-ku Yokohama 226-8503, Japan, and <sup>e</sup>High Energy Accelerator Research Organization, Institute of Materials Structure Science, Oho 1-1 Tsukuba, Ibaraki 305-0801, Japan

Correspondence e-mail:  
tanaka.kiyooki@leto.eonet.ne.jp

Received 10 August 2010  
Accepted 11 February 2011

The crystal structure of mayenite ( $12\text{CaO}\cdot 7\text{Al}_2\text{O}_3$ ) has been investigated by single-crystal synchrotron diffraction with high resolution and accuracy, using a four-circle diffractometer equipped with an avalanche photodiode detector (APD) detector installed at PF14A in Tsukuba, Japan. Analysis revealed random displacements of ions by the electrostatic force of the  $\text{O}^{2-}$  ion (O3) clathrated in two out of 12 cages. O3 ions are located at general positions close to the  $\bar{4}$  site at the centre of each cage. The difference-density map revealed two large peaks corresponding to displaced Ca ions. The positive ions close to O3 are displaced and one-to-one correspondence was found between one of the four equivalent O3 ions and the displaced ions. When an O3 ion is present in the cage the Al ion at the 16c position moves 0.946 (3) Å toward the O3 ion. One of the Al–O bonds is broken and a new Al–O3 bond is created. The result is an  $\text{AlO}_4$  tetrahedron that is quite deformed. The three O1 ions and the O2 ion of the destroyed  $\text{AlO}_4$  tetrahedron are forcibly displaced. O1 and O2 have two and one displaced ions, respectively. The local structure of the cage occupied by one of the four O3 ions was determined by calculating the electrostatic potential and electric field in the deformed cage, although the position of one of the displaced O1 ions was not clearly identified.

## 1. Introduction

Mayenite ( $12\text{CaO}\cdot 7\text{Al}_2\text{O}_3$ , hereinafter abbreviated as C12A7) is a well known cement mineral [space group  $I\bar{4}3d$ ,  $a = 11.989$  (3) Å and  $Z = 2$ ]. The unit cell is composed of 12 cages, two of which clathrate an  $\text{O}^{2-}$  ion. Hereinafter the  $\text{O}^{2-}$  ion is referred to as O3; a cage with O3 is termed an occupied cage and that without O3 a vacant one. The occupied cages are distributed so randomly in the crystal that the cubic symmetry is kept. Since O3 lies close to the centre of the cage and is loosely coordinated by cations, it is relatively 'mobile' and C12A7 has a high ionic conductivity due to diffusion of the O3 ions between approximately 773 and 1473 K (Lacerda *et al.*, 1988).

Several interesting properties have been introduced in C12A7 by substituting the O3 ions with other anions such as  $\text{F}^-$  (Jeevaratnam *et al.*, 1964),  $\text{OH}^-$  (Imlach *et al.*, 1971; Li *et al.*, 2005),  $\text{O}_2^-$  (Hosono & Abe, 1987; Matsuishi *et al.*, 2004),  $\text{H}^-$  (Hayashi, Matsuishi *et al.*, 2002),  $\text{O}^-$  (Hayashi, Hirano, Matsuishi & Hosono, 2002) and  $\text{O}_2^{2-}$  (Hayashi *et al.*, 2005). However, in order to extract the O3 ions from the cages C12A7 was treated in a Ca atmosphere and the electric conductivity of C12A7 increased dramatically from  $10^{-10}$  to  $10^2$  S  $\text{cm}^{-1}$  (Matsuishi *et al.*, 2003). This was the first electride (C12A7:e) that is stable at room temperature. It is a metallic

conductor (Matsuishi *et al.*, 2003) and becomes a superconductor at  $\sim 0.4$  K (Miyakawa *et al.*, 2007). These characteristics of C12A7:e are of interest theoretically. The electronic structure has been investigated to obtain a model consistent with these properties (Sushko *et al.*, 2003a,b, 2007; Medvedeva & Freeman, 2004; Li *et al.*, 2004).

The structure of mayenite has been extensively investigated. It was first reported by Bussem & Eitel (1936) using X-ray powder diffraction. However, O3 was not found. Since the crystal has no centre of symmetry and the site occupancy factor (s.o.f.) of O3 is very small, the crystal structure has not yet been fully solved. In the present study the s.o.f. is defined as the probability of finding an atom at the site. Accordingly, when the s.o.f. is multiplied by the number of symmetry-related positions of the site it is equal to the number of ions in the unit cell. O3 was first reported by Bartl & Sheller (1970) as being close to the centre of the cage with point-group symmetry  $\bar{4}$ . Christensen (1987) determined the crystal structure of  $\text{Ca}_{11.3}\text{Al}_{14}\text{O}_{32.3}$  by X-ray diffraction. The crystal structure of C12A7 was measured using the same method at four temperatures between 298 and 1323 K by Boysen *et al.* (2007). A disordered Ca ion was found and the s.o.f.'s of O3 and Ca ions were analysed, although the O3 ions were located at the centre of the cage. The high ionic conductivity was attributed to O3, since the electron density of O3 is spread out at elevated temperatures. The displacement of Ca ions was also reported by Kim *et al.* (2007) using the MEM/Rietveld analysis. Elaborate work on C12A7 and related electriles using neutron and synchrotron powder diffraction has been carried out by Palacios *et al.* (2007). A displacement of Ca, as well as that of O3 from the  $\bar{4}$  position, was found. The displacement of O3 was measured by neutron powder diffraction (Kiyanagi *et al.*, 2008). Owing to the low resolution of the powder diffraction measurements employed in these investigations on C12A7 small displacements of the other ions could not be determined. Using single-crystal synchrotron X-ray diffraction the structures of C12A7 and related electriles were further investigated by Palacios *et al.* (2008) by measuring reflections with  $\sin \theta/\lambda$  up to 1.110; additional displaced ions (one Al and two Ca) were found. O3 was found nearby on a site of  $\bar{4}$  symmetry. Lerch *et al.* (2009) also found one displaced Al ion and one displaced Ca ion. The O3 ion was located at a general position rather than at a  $\bar{4}$  site.

The present study on the structure of C12A7 is the first in our series of investigations on the electrile C12A7:e. Determination of the local structures of the cages in C12A7 is most fundamental since the occupied cages partially remain in C12A7:e and similar distortions are expected. The electron densities of ions displaced by the electrostatic force of O3 and those of electrons clathrated in the cage cannot be distinguished by single-crystal X-ray diffraction. Therefore, all the ion displacements due to O3 in C12A7 should be found before starting an X-ray investigation of the electron density distribution (EDD) of the clathrated electrons. The purpose of the present study is to find all the displaced ions of C12A7 and to understand the local distorted structure to clarify the reasons for the ion displacements.

**Table 1**  
Experimental details.

Crystal data	
Chemical formula	$\text{Al}_{14}\text{Ca}_{12}\text{O}_{33}$
$M_r$	1386.66
Crystal system, space group	Cubic, $I\bar{4}3d$
Temperature (K)	298
$a$ ( $\text{\AA}$ )	11.989 (3)
$V$ ( $\text{\AA}^3$ )	1723.2 (7)
$Z$	2
Radiation type	Synchrotron, $\lambda = 0.67954 \text{ \AA}$
$\mu$ ( $\text{mm}^{-1}$ )	1.99
Crystal size (mm)	$0.07 \times 0.07 \times 0.07 \times 0.03$ (radius)
Data collection	
Diffractometer	Tsukuba BL14A four-circle
Scan method	Integrated intensities from $\omega/2\theta$ scans
Absorption correction	For a sphere <sup>†</sup>
$T_{\min}$ , $T_{\max}$	0.908, 0.909
No. of measured, independent and observed [ $F > 3.0\sigma(F)$ ] reflections	10 790, 3077, 3020
$R_{\text{int}}$	0.012
Refinement	
$R[F^2 > 2\sigma(F^2)]$ , $wR(F^2)$ , $S$	0.016, 0.024, 1.09
No. of reflections	3020
No. of parameters	66
No. of restraints	0
$\Delta\rho_{\max}$ , $\Delta\rho_{\min}$ ( $\text{e \AA}^{-3}$ )	0.34, $-0.39$

Computer programs used: BL14A diffractometer control software (Satow & Iitaka, 1989; Vaalsta & Hester, 1997), *RSLC-3 UNICS* system (Sakurai & Kobayashi, 1979), *sortref*, *gluplot* (Sakakura, 2008), *MOLLY* (Hansen & Coppens, 1978). <sup>†</sup> The transmission coefficient for the spheres tabulated in *International Tables for X-ray Crystallography* (1972, Vol. II, Table 5.3.6B) was interpolated with the Lagrangian method.

## 2. Experimental

Since the O3 ions disturb the electrostatic field the surrounding ions are expected to be displaced. O3 exists randomly in two of the 12 cages and is located at a general position near the  $\bar{4}$  site. Accordingly O3 occupies each position with a probability of  $2/(12 \times 4)$ . Thus, the s.o.f.s of the ions displaced by O3 are expected to be very small so accurate measurement is necessary. Hence intensities up to the highest possible value of  $\sin \theta/\lambda = 1.368 \text{ \AA}^{-1}$  were carefully measured with synchrotron radiation.

Single crystals of mayenite were grown by Czochralski's method. A crystal was shaped into a sphere of diameter 65  $\mu\text{m}$ . Intensities were measured at BL14A of the Photon Factory, Tsukuba, Japan (Satow & Iitaka, 1989), using a four-circle diffractometer equipped with an avalanche photodiode detector (APD), the linearity of which reaches up to  $10^8$  counts  $^{-1}$  (Kishimoto *et al.*, 1998). Polarized synchrotron X-ray beams from a vertical wiggler were selected to  $\lambda = 0.67954 \text{ \AA}$  using double-crystal Si(111) monochromators. The beams were focused using a curved fused-quartz mirror coated with platinum. The Bragg angle of the first Si(111) monochromator and the translation of the second one were adjusted so that the beams pass through a pinhole of diameter 0.4 mm in front of the crystal. Then the plate on which the four-circle diffractometer was placed was rotated around the vertical axis passing through the centre of the incident slit. The base was also translated or inclined vertically so that the beams pass through a pinhole of 0.1 mm diameter. The positions of the

vertical and horizontal half-slits were adjusted manually so that the beams through the pinhole at the crystal position were cut in half and enter an ionic chamber placed at the detector position. After analysis of the pulse heights of the eight channels of the APD detector, deviations from the zero angles of  $2\theta$ ,  $\omega$  and  $\chi$  were calculated by measuring four angles for six reflections of a Si crystal, each at three different positions (King & Finger, 1979). The lattice parameter was calculated to be  $a = 11.989(3) \text{ \AA}$  from  $2\theta$  angles of 24 reflections with  $69.44 \leq 2\theta \leq 72.18^\circ$ . Intensities were then measured up to  $\sin \theta/\lambda = 1.369$  avoiding multiple diffraction (MD). The optimum four angles, where the effect of MD was negligible, were calculated using the  $\varphi$ -scan simulation software *IUANGLE* (Tanaka & Saito, 1975; Tanaka *et al.*, 1994, Takenaka *et al.* 2008). The fluctuation and decay of the incident intensities were monitored by an ionic chamber, and the diffracted intensities were corrected accordingly. Other experimental details are given in Table 1.

### 3. Refinement

The crystal structure of C12A7 is briefly summarized in order to better understand the following discussion. The structure is

**Table 2**  
Symmetry codes.

(0)	$x$ ,	$y$ ,	$z$
(i)	$z$ ,	$-x$ ,	$-y + \frac{1}{2}$
(ii)	$y + \frac{1}{2}$ ,	$z - \frac{1}{2}$ ,	$x + \frac{1}{2}$
(iii)	$-x + \frac{1}{2}$ ,	$y$ ,	$-z + 1$
(iv)	$-x + \frac{3}{4}$ ,	$-z + \frac{1}{4}$ ,	$y + \frac{1}{4}$
(v)	$-z + \frac{3}{4}$ ,	$-y + \frac{1}{4}$ ,	$x + \frac{1}{4}$
(vi)	$-y + \frac{1}{4}$ ,	$-x + \frac{1}{4}$ ,	$z + \frac{1}{4}$
(vii)	$z + \frac{1}{4}$ ,	$y + \frac{1}{4}$ ,	$x + \frac{1}{4}$
(viii)	$-x + \frac{1}{2}$ ,	$-y$ ,	$z + \frac{1}{2}$
(ix)	$y + \frac{3}{4}$ ,	$-x + \frac{1}{4}$ ,	$-z + \frac{3}{4}$
(x)	$-y + \frac{1}{2}$ ,	$-z$ ,	$x + \frac{1}{2}$
(xi)	$-z + \frac{1}{2}$ ,	$-x$ ,	$y + \frac{1}{2}$
(xii)	$x$ ,	$-y$ ,	$-z + \frac{1}{2}$
(xiii)	$-x + \frac{1}{2}$ ,	$-y$ ,	$z - \frac{1}{2}$
(xiv)	$-z + \frac{3}{4}$ ,	$y - \frac{1}{4}$ ,	$-x + \frac{1}{4}$
(xv)	$x + \frac{1}{4}$ ,	$-z + \frac{3}{4}$ ,	$-y + \frac{1}{4}$
(xvi)	$z$ ,	$x$ ,	$y$
(xvii)	$x + \frac{1}{4}$ ,	$z - \frac{3}{4}$ ,	$y + \frac{1}{4}$
(xviii)	$-x + \frac{3}{4}$ ,	$-z - \frac{1}{4}$ ,	$-y + \frac{1}{4}$
(xix)	$-z + 1$ ,	$x - \frac{1}{2}$ ,	$-y + \frac{1}{2}$
(xx)	$-y + \frac{3}{4}$ ,	$x - \frac{1}{4}$ ,	$-z + \frac{3}{4}$
(xxi)	$y + \frac{3}{4}$ ,	$x - \frac{1}{4}$ ,	$z - \frac{1}{4}$
(xxii)	$x + \frac{3}{4}$ ,	$-z + \frac{1}{4}$ ,	$-y + \frac{3}{4}$
(xxiii)	$\bar{y} + 1$ ,	$z - \frac{1}{2}$ ,	$-x + \frac{1}{2}$
(xxiv)	$z + \frac{1}{2}$ ,	$x - \frac{1}{2}$ ,	$y + \frac{1}{2}$
(xxv)	$-z + \frac{3}{2}$ ,	$-x$ ,	$y + \frac{1}{2}$
(xxvi)	$-y$ ,	$z - \frac{1}{2}$ ,	$-x + \frac{1}{2}$
(xxvii)	$-y$ ,	$-z + \frac{1}{2}$ ,	$x$

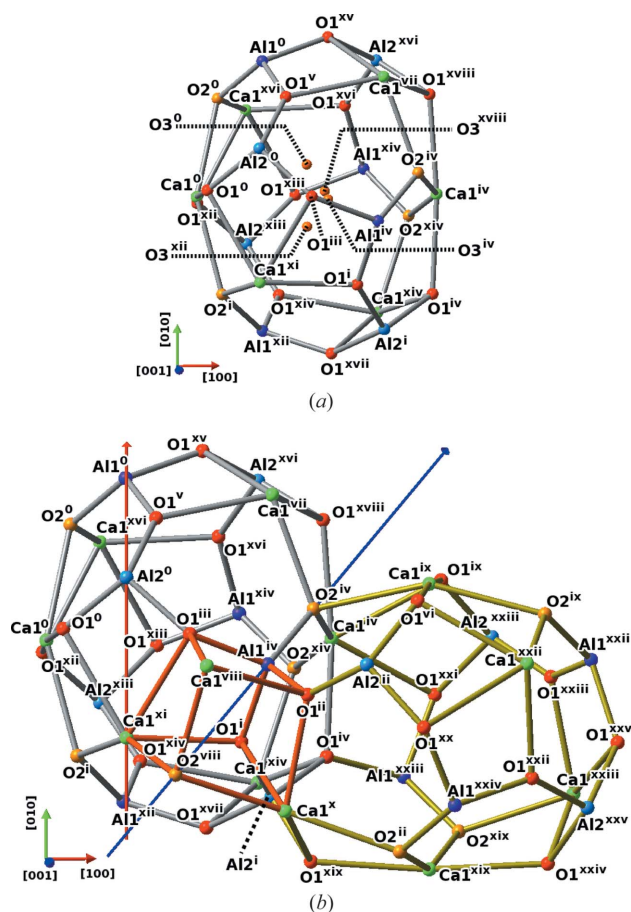


**Figure 1**  
The structure of (a) the vacant cage with its centre at  $(3/8, 0, 1/4)$  and (b) two vacant cages related by the threefold axis in blue. Ca1, Al1, Al2, O1 and O2 ions are drawn as olive, purple, light blue, red and orange balls. Four O3 ions are added in (a) for the sake of comparison.

composed of two types of corner-shared  $\text{AlO}_4$  tetrahedra with Al1 and Al2 at the centre, and Ca counterions. The structure of the vacant cage is illustrated in Fig. 1(a). A picture of the crystal structure showing the arrangement of the cages is deposited as Fig. 9.<sup>1</sup> The symmetry codes are listed in Table 2. Ions in the asymmetric unit have symmetry code '0'. The centre of the cage at  $(3/8, 0, 1/4)$  has point-group symmetry  $\bar{4}$  and is the midpoint of Ca1<sup>0</sup> and Ca1<sup>iv</sup> ions on the 4 axis. The four O3 ions in the cage whose centre is  $(3/8, 0, 1/4)$  are shown in Fig. 1(a). O3 randomly occupies one of four sites  $0.771(8) \text{ \AA}$  from the centre of the cage. Al1 bonds with three O1 ions and one O2, and Al2 bonds with four O1 ions, although the fourth bond is to the O ion in an adjacent cage. In other words each O1 is bonded to Al1 and Al2, while O2 is only bonded to Al1. Bond lengths Al1–O1 and Al2–O1 are  $1.7747(4)$  and  $1.7428(4) \text{ \AA}$ . Fig. 1(b) shows the two cages as being in contact with each other. The two cages are related by a threefold axis (shown in blue) passing through O2<sup>iv</sup>, Al1<sup>iv</sup> and O2<sup>viii</sup>. The distances from O1<sup>i</sup>, O1<sup>ii</sup> and O1<sup>iii</sup> to Ca1<sup>xi</sup>, Ca1<sup>x</sup> and Ca1<sup>viii</sup> are  $2.3500(3) \text{ \AA}$  and those to Ca1<sup>x</sup>, Ca1<sup>viii</sup> and Ca1<sup>xi</sup> are  $2.5143(4) \text{ \AA}$ . Al1 and O2 on the same threefold axis form an Al1–O2 bond of  $1.7342(4) \text{ \AA}$  and the three Ca1 ions are  $2.4148(4) \text{ \AA}$  from O2. The O2<sup>iv</sup> ions are close to Ca1<sup>iv</sup>, Ca1<sup>vii</sup> and Ca1<sup>ix</sup>. Each cage is composed of six Ca1, 12 O1 and four Al1, Al2 and O2 ions; each ion is shared by three cages except Al2 which is shared by four cages. Each cage is surrounded by a further 12 cages. The inner free spaces are connected to eight nearest neighbours *via* six-membered rings

<sup>1</sup> Supplementary data for this paper are available from the IUCr electronic archives (Reference: OG5045). Services for accessing these data are described at the back of the journal.

**Table 3**

Refinements A to I.

$U_{\text{iso}}$  and  $U_{ij}$  are isotropic and anisotropic displacement parameters.

Refinement	Refined coordinates and parameters	R	GOF	Residual peak heights (e Å <sup>-3</sup> ) of ions in parentheses
A	Ca1, Al1, Al2, O1	7.26	6.51	10.0 (Ca1a), 10.8 (Ca1b)
B	Ca1a, Ca1b	3.89	3.70	1.54 (Al1a)
C	Al1a	3.17	2.76	1.32 (O3)
D	O3	3.07	2.75	–
E	$P_v$ and $\kappa$ in equation (1)	2.40	2.00	1.40 (O1a)
F	O1a	2.16	1.76	0.84 (Ca1c), 0.71 (O1b)
G	Ca1c, O1b	1.91	1.54	0.53 (Ca1a), –0.76 (Ca1a)
H	Ca1a (displaced from $\bar{4}$ axis)	1.85	1.49	
	O1a, O1b ( $T_{\text{iso}}$ )	1.76	1.42	0.43 (O2a), 0.57 (Ca1b), 0.46 (Al1a)
	O2a, Ca1b ( $T_{ij}$ ), Al1a ( $T_{\text{iso}}$ )	1.70	1.35	
I	$P_v$ of Al1a	1.61	1.09	–0.39 < $\Delta\rho$ < 0.34

of diameter  $\sim 1 \text{ \AA}$ , such as  $\text{O2}^{\text{iv}}-\text{Al1}^{\text{iv}}-\text{O1}^{\text{i}}-\text{Al2}^{\text{i}}-\text{O1}^{\text{iv}}-\text{Ca1}^{\text{iv}}$ , and to the remaining four cages *via* four-membered rings, such as  $\text{Al2}^{\text{0}}-\text{O1}^{\text{0}}-\text{Ca1}^{\text{xi}}-\text{O1}^{\text{iii}}$ .  $\text{Al2}^{\text{0}}$  and  $\text{Ca1}^{\text{xi}}$  are on the  $\bar{4}$  axis in red. The box written in orange lines is composed of six four-membered rings such as  $\text{Al1}^{\text{iv}}-\text{O1}^{\text{iii}}-\text{Ca1}^{\text{xi}}-\text{O1}^{\text{i}}$ .

The program *MOLLY* (Hansen & Coppens, 1978) was used in the present study for multipole refinement. The electron density  $\rho_{\text{at}}$  of each atom was expressed as the sum of the electron density of the core electrons  $\rho_{\text{core}}(r)$  and the valence electrons  $\rho_{\text{valence}}(\kappa r)$

$$\rho_{\text{at}}(r) = \rho_{\text{core}}(r) + P_v \kappa^3 \rho_{\text{valence}}(\kappa r), \quad (1)$$

where  $P_v$  is the population coefficient and  $\kappa$  expresses the expansion ( $\kappa < 1$ ) or contraction ( $\kappa > 1$ ) of  $\rho_{\text{atomic}}(r)$  (Coppens *et al.*, 1979). Since a prominent aspherical EDD was not observed for ionic bonds in C12A7, parameters describing the aspherical EDD and anharmonic thermal vibrations were not refined. Scattering factors were calculated using the radial functions from Clementi & Roetti (1974). The valence electron configuration ( $3p^6$  for  $\text{Ca}^{2+}$  and  $2p^6$  for  $\text{Al}^{3+}$  and  $\text{O}^{2-}$ ) was initially assumed. They describe a spherical EDD around each ion. Anomalous dispersion terms were calculated by interpolating the values presented by Chantler (1995, 2000).

### 3.1. Refinement A of the vacant cage

Since the crystal has no centre of symmetry, the phase of each reflection takes an actual value between 0 and  $2\pi$ . When the structure is not well determined, the phases are not fixed well so that there are sometimes ghost peaks in the difference density  $\Delta\rho(\mathbf{r})$  at places where no chemical entity exists.  $\Delta\rho(\mathbf{r})$  is defined as

$$\Delta\rho(\mathbf{r}) = \frac{1}{V} \sum_{\mathbf{h}} (F_o(\mathbf{h}) - F_c(\mathbf{h})) \exp(-2\pi i \mathbf{h} \cdot \mathbf{r}), \quad (2)$$

where  $F_o$  and  $F_c$  are observed and calculated structure factors,  $\mathbf{h}$  is the reciprocal vector, and  $V$  is the volume of the unit cell. Therefore, only the displaced ion having the largest peak in the difference-density map after each step of the least-squares refinement was added in the subsequent step. When the peak could be removed without producing ghost peaks and the  $R$  factors were significantly reduced, the ion was accepted as a correct feature of the structure. In the present study displaced ions are noted by adding  $a$ ,  $b$  or  $c$  to the label of the ion in the vacant cage. The newly added ions as well as the  $R$  factors, GOFs and maximum peak heights in the difference-density map in each stage of the refinement are listed in Table 3.

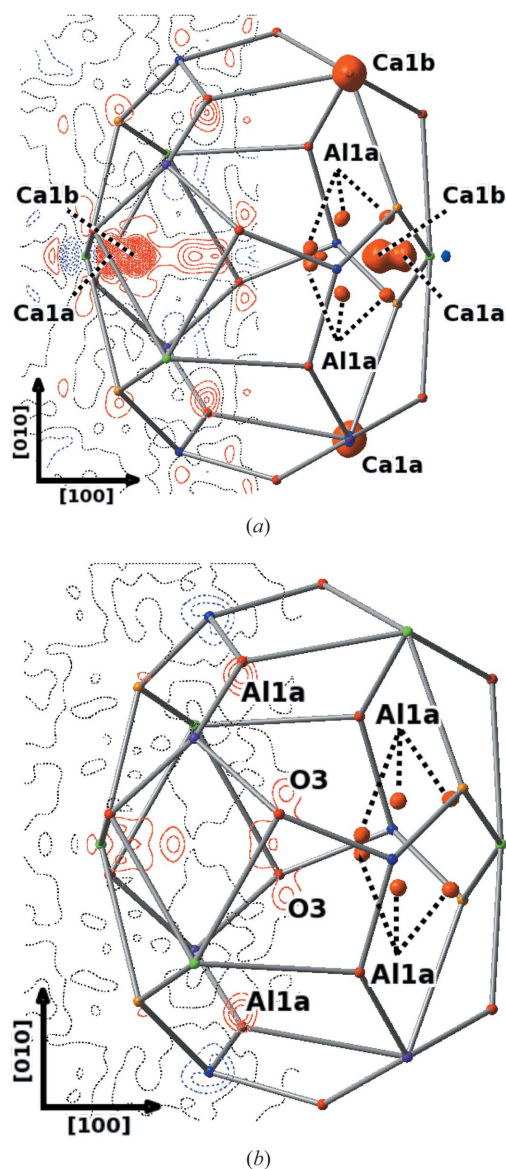


**Figure 2** Difference density on the  $z = 1/4$  plane including the  $\bar{4}$  axis after (a) refinement A and (b) refinement B. Contours on the left are at  $1.0 \text{ e \AA}^{-3}$ . The surface of constant charge density is shown on the right at  $2.0 \text{ e \AA}^{-3}$ . The right side of the figure is transformed from the left by 4. Red and blue indicate positive and negative densities. No peak is found at  $(3/8, 0, 1/4)$ , the centre of the cage.

The initial atomic positions were taken from the previous study (Bartl & Sheller, 1970). All ions except O3 were included in refinement A. No extinction effect was observed in the present study, probably because the distortion of the crystal structure caused by O3 lowers the crystallinity. The  $R$  factor defined as  $\Sigma(|F_o| - |F_c|)/\Sigma|F_o|$  is 0.0726 and the GOF is 6.51. The difference density is shown in Fig. 2(a). It is striking that two almost equivalent peaks of 10.0 and 10.8 e Å<sup>-3</sup> appear near Ca1 on the  $\bar{4}$  axis between Ca1<sup>0</sup> and Ca1<sup>iv</sup>. These peaks are due to the displaced ions of the two Ca1 ions attracted toward O3 near the centre of the cage. They are numbered Ca1a and Ca1b. Ca1a and Ca1b lie 0.369 (2) and 0.8102 (15) Å from Ca1 toward O3. Recently Palacios *et al.* (2008) also found the second peak.

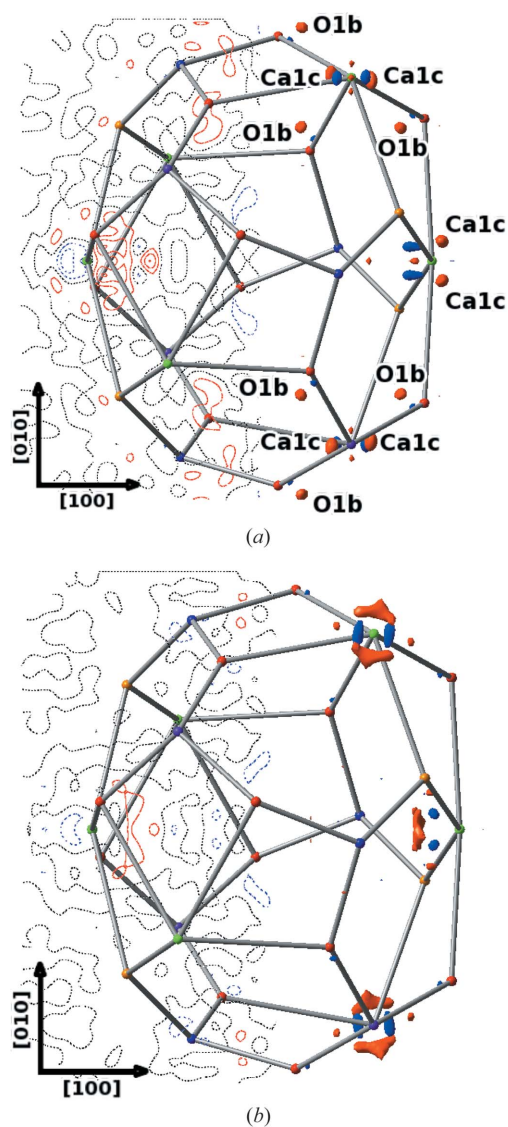


**Figure 3**  
Difference density after (a) refinement F and (b) refinement I. Contours at 0.5 e Å<sup>-3</sup>. Surface of constant charge density at (a) ±0.55 e Å<sup>-3</sup> and (b) ±0.28 e Å<sup>-3</sup>.

### 3.2. Refinements B, C and D: determination of the position of Ca1a, Ca1b, Al1a and O3

Ca1a and Ca1b were included in refinement B. The s.o.f.s of Ca1a and Ca1b converged to 0.076 (3) and 0.070 (2), which are close to  $2 \times (1/24) \doteq 0.0833$ . An isotropic displacement factor equivalent to the anisotropic displacement factor of Ca1 was applied to Ca1a and Ca1b. The values of  $R$  and GOF are 0.0389 and 3.70. The large peaks of Ca1a and Ca1b in Fig. 2(a) are deleted in Fig. 2(b) after refinement B. The large peak on the  $\bar{4}$  axis between Ca1b and O3 in Fig. 2(a) is a ghost one, since it disappeared in Fig. 2(b) after improving the phases of reflections by including Ca1a and Ca1b in the refinement. The largest peaks of 1.54 e Å<sup>-3</sup> are in close proximity to Al1 (see Fig. 2b). These peaks were taken into account in refinement C as Al1a; the s.o.f. of Al1a converged to 0.041 (2) and the peaks disappeared. At the same time, residual peaks of 1.32 e Å<sup>-3</sup> remained near the centre of the cage. These peaks were assigned as O3 ions and included in refinement D, keeping the s.o.f. of O3 at 1/24. They were deleted in the difference-density map after refinement D.<sup>2</sup>

### 3.3. Restriction on s.o.f. of displaced ions

In previous refinements it was evident that the s.o.f. of the displaced ions and O3 have the following approximate relationship

$$\begin{aligned} \text{s.o.f.}(\text{Ca1a}) : \text{s.o.f.}(\text{Ca1b}) : \text{s.o.f.}(\text{Al1a}) : \text{s.o.f.}(\text{O3}) \\ \doteq 2 : 2 : 1 : 1. \end{aligned} \quad (3)$$

Since the Ca1a and Ca1b ions are still on the  $\bar{4}$  axis, the two O3 ions related by a twofold axis coincident with the  $\bar{4}$  axis affect the Ca1 ion on the axis equally. Accordingly, the s.o.f.s of Ca1a and Ca1b are twice those of the other ions. Multiplication of the s.o.f. by the number of symmetry-related positions leads to the following relation

$$n(\text{Ca1a}) : n(\text{Ca1b}) : n(\text{Al1a}) : n(\text{O3}) \doteq 1 : 1 : 1 : 1, \quad (4)$$

where  $n(X)$  is the total number of  $X$  ions in the unit cell. When O3 enters into a vacant cage and occupies a general position the original crystallographic symmetries of the displaced ions close to it are lost locally but the one-to-one correspondence between their s.o.f.s and that of O3 remains. Consequently, the s.o.f. of each displaced ion was expected to be an integer multiple of that of O3. Since the total number of O3 ions at the 48e position is two, the s.o.f. of O3 becomes 2/48 and those of all the displaced ions were fixed to satisfy (4) in the following refinement. The validity of the assumption will be discussed in §4.3.

### 3.4. Refinement E to I for additional displaced ions

$P_v$  and  $\kappa$  in (1) were refined to  $R = 0.0240$  and the peaks remained close to O1a in refinement E. Significant peaks of 0.84 e Å<sup>-3</sup> were left above and below Ca1 in Fig. 3(a) after refinement F. These peaks are due to Ca1c. Significant peaks

<sup>2</sup> Difference-density map after refinements C, D, E, G and H are deposited as Figs. 10, 11, 12, 13, 14.

**Table 4**

Atomic parameters, s.o.f.s and final valence parameters.

(a) Final atomic parameters and s.o.f.s (anisotropic displacement parameters of Ca1, Al1, Al2, O1, O2 and Ca1b are deposited as Table 4c). Isotropic displacement parameters  $U_{\text{iso}}$  are given for displaced ions except Ca1b; others are refined with the anisotropic displacement parameters.

Atom	S.o.f.	<i>x</i>	<i>y</i>	<i>z</i>	$U_{\text{iso}}$ (Å <sup>2</sup> )
Ca1 <sup>0</sup>	3/4	0.139339 (15)	0	1/4	0.00869 (2)
Al1 <sup>0</sup>	7/8	0.268614 (9)	= <i>x</i>	= <i>x</i>	0.00633 (2)
Al2 <sup>0</sup>	1	1/4	1/8	1/2	0.00679 (3)
O1 <sup>0</sup>	11/12	0.15052 (4)	0.036055 (3)	0.442343 (3)	0.01155 (5)
O2 <sup>0</sup>	7/8	0.18510 (4)	= <i>x</i>	= <i>x</i>	0.01011 (5)
Ca1a <sup>0</sup>	1/24	0.16936 (16)	0.00673 (17)	0.25038 (24)	0.00987 (16)
Ca1b <sup>0</sup>	1/12	0.20692 (12)	0	1/4	0.01277 (18)
Ca1c <sup>0</sup>	1/24	0.13537 (17)	0.00426 (29)	0.23538 (22)	= Ca1
Al1a <sup>0</sup>	1/24	0.30406 (23)	0.19844 (24)	0.26186 (23)	0.0096 (3)
O1a <sup>0</sup>	1/24	0.1302 (3)	0.0603 (3)	0.43286 (28)	0.0039 (3)
O1b <sup>0</sup>	1/24	0.1718 (5)	0.0312 (4)	0.4352 (5)	0.0079 (6)
O2a <sup>0</sup>	1/24	0.1996 (6)	0.1750 (7)	0.1893 (6)	= O2
O3 <sup>0</sup>	1/24	0.3559 (6)	0.0614 (7)	0.2506 (7)	0.0163 (8)

(b) Final valence parameters *P<sub>v</sub>* and  $\kappa$ . Parameters of the displaced ions are fixed to those of the ions in the vacant cage.

Atom	Ca1	Al1	Al2	O1	O2	O3
<i>P<sub>v</sub></i>	6.50 (11)	6.32 (5)	6.20 (5)	5.63 (7)	5.90 (9)	6.0
$\kappa$	1.021 (6)	0.985 (5)	0.980 (5)	0.869 (6)	0.880 (9)	1.0

of 0.71 e Å<sup>-3</sup> also exist near O1 and the displaced ion is named O1b. These peaks were deleted in refinement G, including Ca1c and O1b, and the *R* factors decreased from 0.0216 to 0.0191, as listed in Table 3. Positive peaks of 0.53 e Å<sup>-3</sup> remain above and below Ca1a, and a negative peak of -0.76 e Å<sup>-3</sup> still exists on Ca1a. Thus, Ca1a was further displaced from the  $\bar{4}$  axis in refinement H, and these peaks were deleted. Since the s.o.f.s of the displaced ions are very small, the same isotropic displacement parameters of those of the corresponding ions in the vacant cage were applied. However, independent isotropic displacement factors were assigned to O1a, O1b and Al1a in refinement H reducing the *R* factor to 0.0176. Also, three peaks due to O2a displaced from O2 on a threefold axis were found and included in the refinement. Anisotropic and isotropic displacement parameters of Ca1b and Al1a were then refined independently of those for Ca1 and Al1.

The refinement revealed the displaced ions Ca1a, Ca1b, Ca1c, Al1a, O1a, O1b and O2a, while Al2 has no displaced ion. The electron population *P<sub>v</sub>* of Al1a was finally added in refinement I reducing the *R* factor to 0.016. The final atomic parameters after refinement I and the orbital parameters in (1) are listed in Tables 4(a) and (b).<sup>3</sup> The residual density map is shown in Fig. 3(b). The maximum height and depth of the peaks are 0.34 and -0.39 e Å<sup>-3</sup> around the Ca1 ions. The residual density at the centre of the cage is -0.08 e Å<sup>-3</sup> indicating no ion exists there.

## 4. Results and discussion

The ion displacement caused by O3 at its four equivalent positions related by the  $\bar{4}$  operation at (3/8, 0, 1/4) are over-

<sup>3</sup> Anisotropic displacement parameters are deposited as Table 4(c).

**Table 5**

Al—O distances (Å) from Al1a<sup>iv</sup>.

Al1—O1, Al1—O2 and Al2—O1 are 1.7747 (4), 1.7342 (4) and 1.7428 (4) Å.

Distance from Al1a <sup>iv</sup> (Å)	
O1 <sup>i</sup>	1.673 (3)
O1a <sup>i</sup>	1.431 (5)
O1b <sup>i</sup>	1.937 (8)
O1 <sup>ii</sup>	2.709 (3)
O1a <sup>ii</sup>	2.658 (5)
O1b <sup>ii</sup>	2.936 (7)
O1 <sup>iii</sup>	1.839 (3)
O1a <sup>iii</sup>	1.899 (5)
O1b <sup>iii</sup>	2.051 (7)
O2 <sup>iv</sup>	1.705 (3)
O2a <sup>iv</sup>	1.551 (8)
O2a <sup>v</sup>	1.726 (9)
O2a <sup>vi</sup>	1.722 (9)
O3 <sup>iv</sup>	1.762 (9)

lapped because of the high cubic symmetry. Therefore, the next step of the crystal structure analysis is to construct the structure of the cage occupied by one of the four O3 ions. In other words, actual displaced ions in the occupied cage were selected from the list of displaced ions in Table 4(a).

### 4.1. Occupied cage structure constructed from the displaced ions

Since Al1<sup>iv</sup> is the closest ion to O3<sup>iv</sup> and large peaks of Al1a remain in Fig. 2(b), Al1<sup>iv</sup> is judged to be shifted to Al1a<sup>iv</sup> by O3<sup>iv</sup> as illustrated in Fig. 4. The distance from Al1<sup>iv</sup> to Al1a<sup>iv</sup> is 0.946 (3) Å. Distances from Al1a<sup>iv</sup> to the surrounding O ions are listed in Table 5. Al1<sup>iv</sup> moves toward O1<sup>i</sup> and O2<sup>iv</sup> but away from O1<sup>ii</sup> and O1<sup>iii</sup>. It also becomes evident that the shift breaks the Al1<sup>iv</sup>—O1<sup>ii</sup> bond and allows the formation of a new Al1a<sup>iv</sup>—O3<sup>iv</sup> bond of 1.762 (9) Å. Since the angles of O3<sup>iv</sup>—Al1<sup>iv</sup>—O1<sup>ii</sup> and O3<sup>iv</sup>—Al1a<sup>iv</sup>—O1b<sup>ii</sup> are 169.27 (18) and 171.9 (3)°, O1<sup>ii</sup>, Al1<sup>iv</sup>, Al1a<sup>iv</sup> and O3<sup>iv</sup> lie on a nearly straight

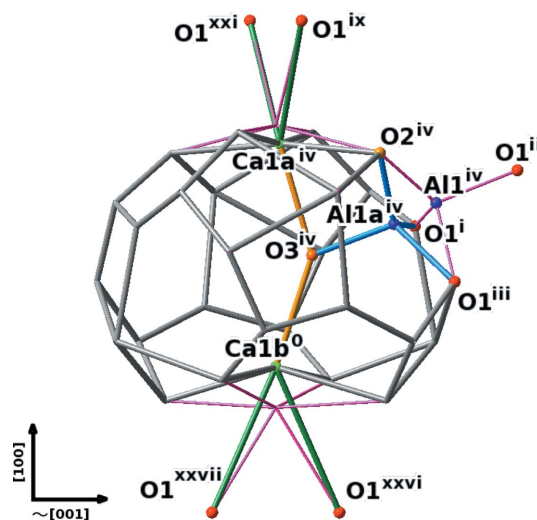


**Figure 4**

Relationship of the vacant and occupied cages with O3<sup>iv</sup> and displaced Al1 and Ca1 ions. Thin pink lines show the vacant cage.

line. The conformations of the two tetrahedra of  $\text{Al1}^{\text{iv}}-\text{O1}^{\text{i}}-\text{O1}^{\text{ii}}-\text{O1}^{\text{iii}}-\text{O2}^{\text{iv}}$  and  $\text{Al1a}^{\text{iv}}-\text{O1}^{\text{i}}-\text{O3}^{\text{iv}}-\text{O1}^{\text{iii}}-\text{O2}^{\text{iv}}$  are almost enantiomorphic, as shown in Fig. 4.

The shift of  $\text{Al1}^{\text{iv}}$  to  $\text{Al1a}^{\text{iv}}$  gives rise to electrostatic repulsions among the oxygen ions of the  $\text{Al1}^{\text{iv}}\text{O}_4$  tetrahedron, and they are expected to be displaced. Since the attractive force from  $\text{Al1}^{\text{iv}}$  is lost,  $\text{O1}^{\text{ii}}$  is expected to be displaced toward  $\text{Al2}^{\text{ii}}$ . The distances of  $\text{Al2}^{\text{ii}}$  to  $\text{O1a}^{\text{ii}}$  and  $\text{O1b}^{\text{ii}}$  are 1.820 (4) and 1.657 (6) Å, which is longer and shorter than the  $\text{Al2}-\text{O1}$  bond [1.7428 (4) Å]. Accordingly,  $\text{O1}^{\text{ii}}$  is expected to be displaced to  $\text{O1b}^{\text{ii}}$ , which is closer to  $\text{Al2}^{\text{ii}}$ . However, a simple comparison of the distances in Table 5 does not identify the other displaced ions around  $\text{Al1a}^{\text{iv}}$ . Therefore, the electrostatic

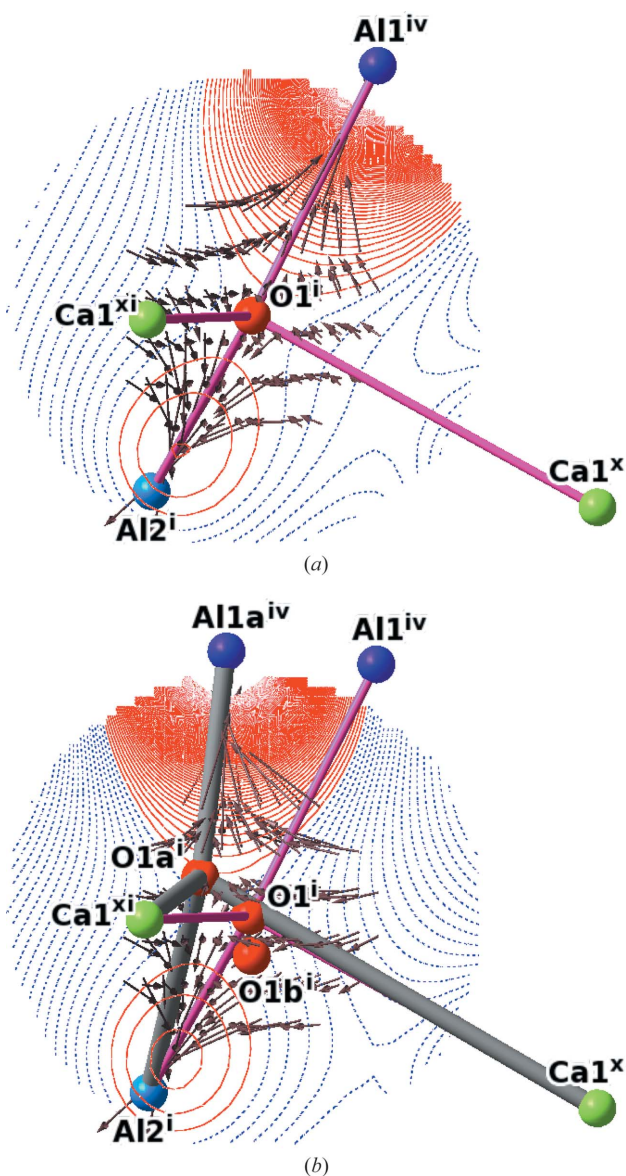


**Figure 5** Potential and negative electric field around  $\text{O1}^{\text{i}}$  in (a) the vacant and (b) the occupied cages on the plane of  $\text{Al1}^{\text{iv}}$ ,  $\text{O1}^{\text{i}}$  and  $\text{Al1a}^{\text{iv}}$ . Red solid contours are positive and blue broken ones are negative. The contours are at  $0.2 \text{ e } \text{Å}^{-1}$ . The arrows indicate the direction and strength of the electric field acting on a negative unit charge. For details see text.

**Table 6** Distances (Å) of the ions around  $\text{O3}^{\text{iv}}$  up to 3.5 Å in an occupied cage.

Distance from $\text{O3}^{\text{iv}}$ (Å)	
$\text{Al1a}^{\text{iv}}$	1.762 (9)
$\text{Ca1b}^{\text{iv}}$	1.932 (8)
$\text{O1a}^{\text{i}}$	2.235 (9)
$\text{Ca1a}^{\text{iv}}$	2.331 (8)
$\text{Ca1b}^{\text{0}}$	2.361 (8)
$\text{O2a}^{\text{iv}}$	2.430 (11)
$\text{Ca1a}^{\text{0}}$	2.793 (8)
$\text{O1}^{\text{v}}$	2.972 (9)
$\text{O1}^{\text{iii}}$	3.032 (8)
$\text{Al2}^{\text{0}}$	3.219 (8)
$\text{Ca1}^{\text{xi}}$	3.219 (9)
$\text{Al2}^{\text{i}}$	3.336 (9)
$\text{O1}^{\text{0}}$	3.344 (8)
$\text{O1}^{\text{iv}}$	3.382 (8)
$\text{Ca1}^{\text{vii}}$	3.393 (9)

potential and electric field around  $\text{O1}^{\text{i}}$ ,  $\text{O1}^{\text{iii}}$  and  $\text{O2}^{\text{iv}}$ , as well as  $\text{O1}^{\text{ii}}$  were calculated to determine the local structure.

#### 4.2. Electrostatic potential

Since the covalent character of the bonds is small in C12A7, the possible direction of the displacement of an ion can be estimated from the difference of the electrostatic potentials of the occupied and vacant cages. The electrostatic potential,  $V_n(\mathbf{r})$ , of the  $n$ th ion at  $\mathbf{R}_n$  is expressed as

$$V_n(\mathbf{r}) = \sum_{m \neq n} \frac{Z_m}{|\mathbf{r} - \mathbf{R}_m|} - \int \frac{\rho'(\mathbf{r}')}{|\mathbf{r} - \mathbf{r}'|} d\mathbf{r}', \quad (5)$$

where  $Z_m$  is the atomic number of the  $m$ th ion. The variable  $\rho'(\mathbf{r}')$ , which denotes the superposition of all the atomic electron densities at  $\mathbf{r}'$  except that of the  $n$ th ion, was calculated using the final parameters after refinement I with the program *StoPot* (Sakakura, 2008). The potential was calculated under the following rules:

(i) Ions within 17 Å of the  $n$ th ion are included in the potential calculation.

(ii) Cages sharing the  $n$ th ion in (5) were assumed to have no  $\text{O3}$  ion and  $1/6 \text{ O}^{2-}$  ions were placed at the centre of all the other cages.

(iii)  $\text{O3}$  and the ions displaced by  $\text{O3}$  were included in the calculation.

(iv) When the  $n$ th ion is not a member of the occupied cage,  $1/6 \text{ O}^{2-}$  and  $\text{O3}$  may be placed together in the cage according to rule (ii). In this case the  $1/6 \text{ O}^{2-}$  ions were removed.

When rule (ii) is applied three or four cages are vacant at any one time since each ion is shared by three or four cages. The probability of all the eight nearest-neighbour cages around the occupied cage not having  $\text{O3}$  is only  $(5/6)^8 = 0.23$ , since crystal symmetry demands that all the cages should have an  $\text{O}^{2-}$  ion with a probability of  $1/6$ . On the other hand, the probability of having three or four vacant cages at a time is  $(5/6)^3 = 0.58$  or  $(5/6)^4 = 0.48$ . Accordingly rule (ii) is more appropriate than a model with the occupied cage surrounded by vacant cages.

The local structure of the cage which has  $O3^{iv}$  at a general position near the centre,  $(3/8, 0, 1/4)$ , was selected for more careful examination. Since the structure was not yet known, the initial configuration of the ions must be selected carefully. The potential of the ion closest to  $O3^{iv}$  was first determined. The distances from  $O3^{iv}$  to the surrounding ions up to  $3.5 \text{ \AA}$  are listed in Table 6. When one of the displaced ions was specified it was included in the following calculation. In this way the displaced ions were consecutively specified and the potential improved.

**4.2.1. Ca1a and Ca1b in the occupied cage.** Since the peaks of Ca1a and Ca1b on the difference-density map are very large and displacements from Ca1 to Ca1a and Ca1b are larger than those of O ions, they are discussed first.  $Ca1^0$  and  $Ca1^{iv}$  lie closer to  $O3^{iv}$  than the other Ca1 ions and are expected to be shifted to one of the two displaced positions, that is to Ca1a or Ca1b. Since the heights of the peaks of Ca1a and Ca1b are nearly equal in Fig. 1(a), the two types of displacement occur with equal probability. Also the 1:1 correspondence of the displacements described in §3.3 requires  $Ca1^0$  and  $Ca1^{iv}$  to be shifted differently. Therefore, only two models of the displacements are possible. One model involves the displacement of  $Ca1^{iv}$  and  $Ca1^0$  to  $Ca1a^{iv}$  and  $Ca1b^0$ . Another model involves displacements to  $Ca1b^{iv}$  and  $Ca1a^0$ . The ionic radii of  $Ca^{2+}$  and  $O^{2-}$  are 1.0 and 1.38 Å (Shannon & Prewitt, 1969). In Table 6 the distances from  $O3^{iv}$  to  $Ca1a^{iv}$  and  $Ca1b^0$  are 2.331 (8) and 2.361 (8) Å, while those to  $Ca1b^{iv}$  and  $Ca1a^0$  are 1.932 (8) and 2.793 (8) Å. Since  $Ca1b^{iv}-O3^{iv}$  is shorter and  $Ca1a^0-O3^{iv}$  is longer than the sum of the ionic radii (2.38 Å), the former is judged to be the real structure.<sup>4</sup> The displaced Ca1a ion was first reported by Palacios *et al.* (2008), who also reported that many of the O3 ions are still located at the centre of the cage where none were detected in the present study.

**4.2.2. O1a, O1b and O2a in the occupied cage.** The potentials defined in equation (5) for vacant and occupied cages around  $O1^i$  are shown in Figs. 5(a) and (b). For the sake of simplicity the potential is illustrated so that it becomes zero at (a)  $O1^i$  and (b)  $O1a^i$  by subtracting the potential at each position. The magnitude and direction of the electrostatic force that acts on the unit negative charge, which we call a negative electric field, is also illustrated by arrows with arbitrary scale. The potential in the vacant cage in Fig. 5(a) is properly calculated, since the negative  $O1^i$  ion is located at the saddle point of the positive potential and is attracted towards  $Al1^{iv}$  and  $Al2^i$ . These Al ions have larger positive charges than the Ca1 ions and are located closer to  $O1^i$  than the Ca1 ions. The negative  $O1a^i$  ion in Fig. 5(b) lies close to the saddle point of the positive potential between the two Al ions and is strongly attracted to  $Al1a^{iv}$ , while  $O1b^i$  is in a lower potential area and is attracted more by  $Al2^i$  whilst being displaced in the opposite direction to that specified by the attractive force of  $Al1a^{iv}$ . Therefore, the  $O1a^i-Al1a^{iv}$  bond in Table 5 is judged to exist in the local structure, although the length of the  $Al1a^{iv}-O1a^i$  bond [1.431 (5) Å] is significantly shorter than

<sup>4</sup> The two models are illustrated in Figs. 15 and 16 of the supplementary material.

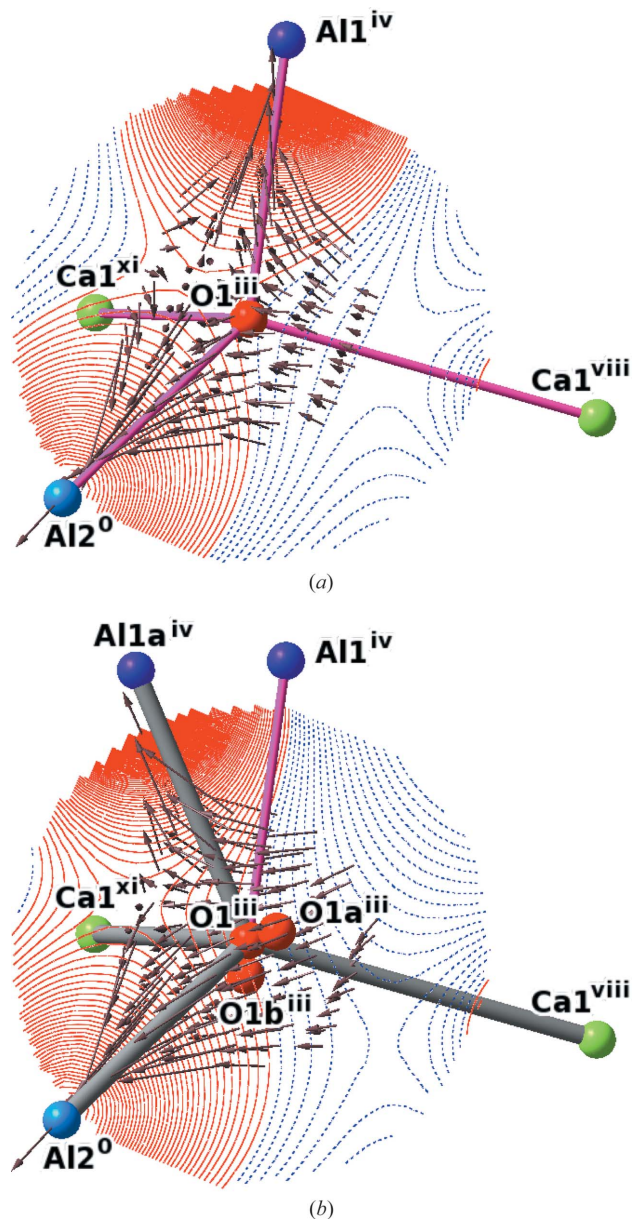


**Figure 6** Potential around  $O1^{iii}$  on the plane of  $Al1^{iv}$ ,  $Al1a^{iv}$  and  $O1^{iii}$  in (a) vacant and (b) occupied cages. The potential at  $O1^{iii}$  is subtracted. Contours are as in Fig. 5.

1.77 Å, which is the sum of the ionic radii of sixfold coordinated  $Al^{3+}$  and  $O^{2-}$ .

In a similar way  $O1b^{ii}$  and  $O2a^{iv}$  are judged to exist in the occupied cage.  $O1b^{ii}$  was already judged to be bonded to  $Al2^{ii}$  in §4.1. Since  $O1b^{ii}$  and  $O2a^{iv}$  only bond to  $Al2^{ii}$  and  $Al1a^{iv}$ , all the arrows of the force around them point exclusively to them. The breaking of the  $Al1^{iv}-O1^{ii}$  bond is also seen in figures of the potentials.<sup>5</sup>  $Al1a^{iv}$  is 2.936 (7) Å from  $O1b^{ii}$ , as seen in Table 5, but is still one of its four nearest neighbours. Thus,  $O1b$  is relatively free and the isotropic displacement parameter,  $U_{iso}$ , of  $O1b$  is twice that of  $O1a$  in Table 4(a).

<sup>5</sup> Those around  $O2a^{iv}$  have been deposited as Figs. 19 and 20.

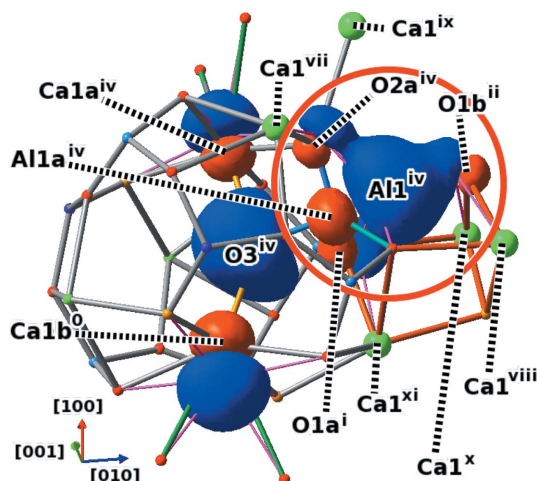


**Figure 7**

Difference in potential of the occupied and vacant cages. The equipotential surface is at  $\pm 3.70 \text{ e \AA}^{-1}$ . The  $\text{Al1}^{\text{iv}}$  area in the red circle exhibits the maximum difference.

The potential in the vacant cage around  $\text{O1}^{\text{iii}}$ , and that around  $\text{O1a}^{\text{iii}}$  and  $\text{O1b}^{\text{iii}}$  on the plane of  $\text{Al1}^{\text{iv}}$ ,  $\text{Al1a}^{\text{iv}}$  and  $\text{O1}^{\text{iii}}$ , is illustrated in Figs. 6(a) and (b), rescaling the potential at  $\text{O1}^{\text{iii}}$  to zero.  $\text{O1a}^{\text{iii}}$  and  $\text{O1b}^{\text{iii}}$  are not on the plane but deviate  $-0.347$  and  $0.153 \text{ \AA}$  along the normal plane. Since the distances from  $\text{Al1a}^{\text{iv}}$  to  $\text{O1a}^{\text{iii}}$  and  $\text{O1b}^{\text{iii}}$  in Table 5 are significantly longer than the  $\text{Al1}^{\text{iv}}-\text{O1}^{\text{iii}}$  bond,  $\text{O1a}^{\text{iii}}$  and  $\text{O1b}^{\text{iii}}$  are attracted by  $\text{Al2}^{\text{o}}$ . In fact, the force acting on them in Fig. 6(b) is directed toward  $\text{Al2}^{\text{o}}$ . Since  $\text{O1b}^{\text{iii}}$  is attracted toward  $\text{Al2}^{\text{o}}$  and the potential at  $\text{O1b}^{\text{iii}}$  is also positive, while that at  $\text{O1a}^{\text{iii}}$  is negative and is located away from  $\text{Al2}^{\text{o}}$ ,  $\text{O1b}^{\text{iii}}$  might be an actual displaced ion. However, since  $\text{O1}^{\text{iii}}$  in Fig. 6(a) and the displaced ions in Fig. 6(b) are located significantly away from the saddle points of the potential, it is also expected that  $\text{O1}^{\text{iii}}$  may not be shifted, or another displaced ion such as  $\text{O1c}$  may be found around the saddle point of the potential in Fig. 6(b).

Since no displacement of  $\text{Al2}$  was found,  $\text{Al2}$  was not affected by the newly formed bonds  $\text{Al2}^{\text{ii}}-\text{O1b}^{\text{ii}}$  and  $\text{Al2}^{\text{o}}-\text{O1b}^{\text{iii}}$  with bond lengths of  $1.657$  (6)  $\text{ \AA}$ , which is shorter than the sum of the ionic radii.

**4.2.3. Ca1c in the local structure.** As stated in §3.4, the peaks of  $\text{Ca1c}$  shown in Fig. 3(a) are significant. The two  $\text{Ca1c}$  peaks near  $\text{Ca1}^{\text{iv}}$ , which is on the extreme right of the horizontal  $\bar{4}$  axis in the middle of the figure, are aligned almost parallel to  $\text{O1}^{\text{iv}}-\text{O1}^{\text{xvii}}$  and perpendicular to  $\text{O2}^{\text{iv}}-\text{O2}^{\text{xiv}}$ . However, since  $\text{Ca1}^{\text{iv}}$  is already displaced to  $\text{Ca1a}^{\text{iv}}$ , it is necessary to find the other Ca1 ions affected by  $\text{O3}$  and to inquire more deeply into the origin of the  $\text{Ca1c}$  peaks. In the vacant cage,  $\text{Ca1}^{\text{viii}}$ ,  $\text{Ca1}^{\text{x}}$  and  $\text{Ca1}^{\text{xi}}$  are located  $3.1369$  (1)  $\text{ \AA}$  from  $\text{Al1}^{\text{iv}}$  on the threefold axis.  $\text{Ca1}^{\text{iv}}$ ,  $\text{Ca1}^{\text{vii}}$  and  $\text{Ca1}^{\text{ix}}$  in Fig. 1(b) are  $3.5809$  (11)  $\text{ \AA}$  from  $\text{Al1}^{\text{iv}}$ .  $\text{Ca1}^{\text{ix}}$  and  $\text{Ca1}^{\text{x}}$  are outside the occupied cage. The possible displacements of these Ca ions excluding  $\text{Ca1}^{\text{iv}}$  are examined.

In order to find the interactions of the Ca1 ions with the local structure, the difference in potentials of the occupied and vacant cages is illustrated in Fig. 7. The most significant

difference is found around  $\text{Al1}^{\text{iv}}$ , followed by the area around the centre of the cage near  $\text{O3}$ . Five Ca1 ions surround the  $\text{Al1}^{\text{iv}}$  area. The potentials of the occupied and vacant cages were calculated using all the displaced ions  $\text{O1a}^{\text{i}}$ ,  $\text{O1b}^{\text{ii}}$ ,  $\text{O2a}^{\text{iv}}$ ,  $\text{Ca1a}^{\text{iv}}$ ,  $\text{Ca1b}^{\text{o}}$  and  $\text{Al1a}$ . The potential and electric field of the

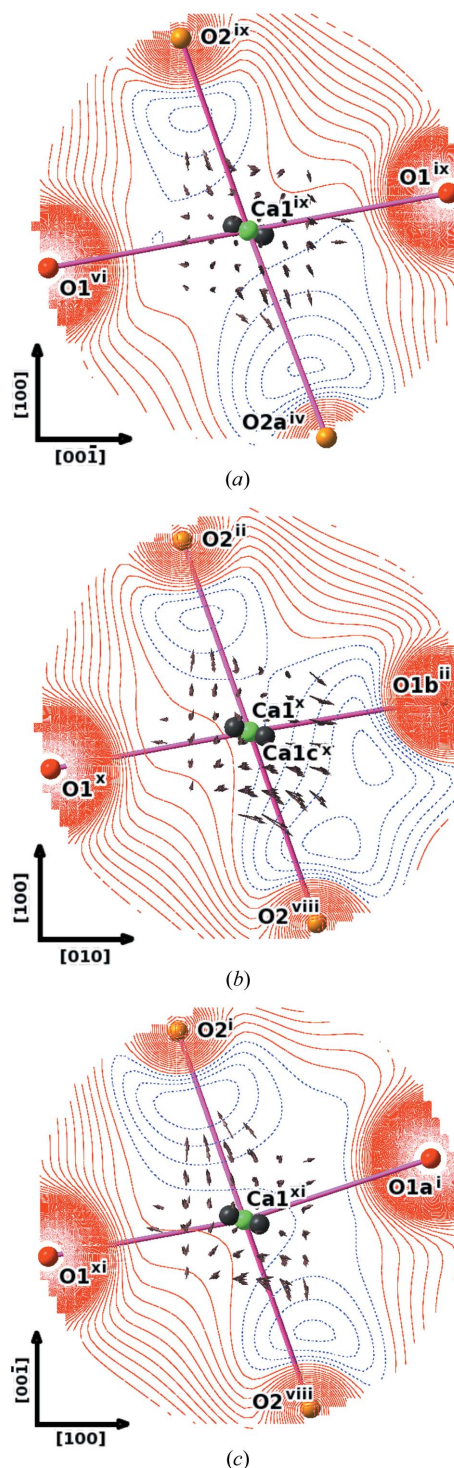


**Figure 8**

Potential on the plane perpendicular to the  $\bar{4}$  axis, including the Ca ion at the centre around (a)  $\text{Ca1}^{\text{ix}}$ , (b)  $\text{Ca1}^{\text{x}}$  and (c)  $\text{Ca1}^{\text{xi}}$  in the occupied cage. The potential of the Ca ion is normalized to zero; contours are as in Fig. 5.  $\text{Ca1c}$  ions are added as dark brown balls.

**Table 7**

Distances (Å) of the Ca1c ions from O3<sup>iv</sup>, Al1a<sup>iv</sup>, Al1<sup>iv</sup> and relevant bonds.

Ca1c	O3 <sup>iv</sup>	Al1a <sup>iv</sup>	Al1 <sup>iv</sup>	Relevant ions
Ca1c <sup>vii</sup>	3.365 (9)	3.313 (4)	3.641 (3)	2.494 (8) (O2a <sup>iv</sup> )
Ca1c <sup>viii</sup>	5.095 (9)	3.577 (4)	2.957 (3)	2.192 (3)† (O1 <sup>iii</sup> )
Ca1c <sup>ix</sup>	5.147 (8)	4.073 (4)	3.641 (3)	2.747 (8) (O2a <sup>iv</sup> )
Ca1c <sup>x</sup>	4.949 (9)	3.544 (4)	2.957 (3)	2.134 (7) (O1b <sup>ii</sup> )
Ca1c <sup>xi</sup>	3.220 (9)	4.968 (4)	2.957 (3)	2.161 (4) (O1a <sup>i</sup> )

† Displaced ion is not specified. Distances from O1a<sup>iii</sup> and O1b<sup>iii</sup> are 2.161 (4) and 2.134 (7) Å.

occupied cage around Ca1<sup>ix</sup>, Ca1<sup>x</sup> and Ca1<sup>xi</sup> are illustrated in Figs. 8(a)–(c).<sup>6</sup> Those of Ca1<sup>x</sup> and Ca1<sup>xi</sup> are similar to those of Ca1<sup>viii</sup> and Ca1<sup>vii</sup>. The distances from these Ca1c ions to O3, Al1a<sup>iv</sup>, Al1<sup>iv</sup> and other relevant ions are listed in Table 7. Ca1<sup>ix</sup> is located at the most stable position, as shown in Fig. 8(a), because of the longer distances from the displaced ions. The distances of Ca1<sup>viii</sup> and Ca1<sup>x</sup> to Al and O ions are similar and those to Al1<sup>iv</sup> are shorter than those of Ca1<sup>vii</sup> and Ca1<sup>ix</sup>. Since the repulsive force of Al1<sup>iv</sup> is lost in the occupied cage, Ca1<sup>x</sup>, for example, is displaced toward Al1<sup>iv</sup> or O1b<sup>ii</sup>. This agrees with the potential in Fig. 8(b) since the (Ca1c<sup>x</sup>)<sup>2+</sup> ion is in contact with the negative potential area along the direction of O1b<sup>ii</sup>. Ca1c<sup>viii</sup> also crosses the negative potential along that to O1<sup>iii</sup>. On the other hand, the directions of the displacement of Ca1<sup>vii</sup> and Ca1<sup>x</sup> are almost parallel to the contour lines, as shown in Fig. 8(c). The repulsive force of Al1<sup>iv</sup> on Ca1c<sup>vii</sup> is compensated for by that of Al1a<sup>iv</sup> in the occupied cage, since the distances of these Al ions to Ca1c<sup>vii</sup> are similar. The distance from Al1<sup>iv</sup> to Ca1c<sup>xi</sup> is the same as those to Ca1c<sup>viii</sup> and Ca1c<sup>x</sup>. However, the distance of Ca1c<sup>xi</sup> to O3 is shorter than that to Al1a<sup>iv</sup>, in contrast to those of Ca1c<sup>viii</sup> and Ca1c<sup>x</sup>. This may be the reason for the different potential of Ca1<sup>xi</sup> from those of Ca1c<sup>viii</sup> and Ca1c<sup>x</sup>. Therefore, it may be concluded that the loss of the repulsive force by Al1<sup>iv</sup> is the main reason for the Ca1c peaks.

### 4.3. Validity of the assumption in the refinement and structure of the occupied cage

The possible local structure of the occupied cage was discussed from a crystallographic viewpoint and from the electrostatic potential and electric field. However, there are several problems still to be investigated since the ratio of the number of occupied to vacant cages is small and the resolution of the experiment may not be high enough.

The constraint in equation (4) corresponding to a 1:1 ratio of displaced ions to one of the four possible positions of O3 worked well since the *R* factor became smallest under the constraint. It does not violate the perfect random distribution of occupied cages required by the cubic crystal symmetry, since it is possible to assume that each cage is randomly occupied by one of the four O3 positions. However, rule (ii) in

<sup>6</sup> Figures of the potential around Ca1<sup>vii</sup> in the vacant cage, and those around Ca1<sup>vii</sup> and Ca1<sup>viii</sup> in the occupied cage have been deposited as Figs. 21, 22 and 23.

§4.2 contradicts the assumption of a perfectly random distribution. However, the potential and electric field calculated with the constraint succeeded in specifying quite clearly the displaced ions, except O1<sup>iii</sup>. Therefore, the rules are acceptable for describing the typical and most probable local structure. Three displaced ions from Ca1, two from O1 and one from each of Al1 and O2 were found in the present study while Al2 at  $\bar{4}$  has no displaced ion. Since the three O1 ions around Al1a<sup>iv</sup> in Table 5 are placed in different electrostatic potential fields, each one should be displaced uniquely. Accordingly, three displaced ions for O1 may be expected. Thus, the third displaced ion may be found as discussed in §4.2.2, although O1<sup>iii</sup> is a tentative candidate of the displaced ion of O1<sup>iii</sup>.

The bond lengths from Al1a<sup>iv</sup> to O1a<sup>i</sup> and O2a<sup>iv</sup> in Table 5 are too short compared with the sum of the ionic radii of the fourfold coordinated O<sup>2-</sup> (1.38 Å) and Al<sup>3+</sup> (0.39 Å), whereas those to O1a<sup>iii</sup> or O1b<sup>iii</sup> are significantly longer than the sum. Accordingly, the Al1a<sup>iv</sup> tetrahedron is extensively deformed. The O3<sup>iv</sup>–Al1a<sup>iv</sup> bond length is 1.762 (9) Å and other close contacts of O3 are 2.331 (8) and 2.361 (8) Å to Ca1a<sup>iv</sup> and Ca1b<sup>0</sup>. The distances of O3<sup>iv</sup> to O1a<sup>i</sup> and O2a<sup>iv</sup> [2.235 (8) and 2.430 Å] are shorter than the sum of the ionic radii of O<sup>2-</sup> (2.74 Å). Thus, the distances to the surrounding oxygen ions suggest that the structure is not stable.

Only the displacements of Ca1, Al1, O1 and O2 ions, which are directly connected to O3, were treated in the present study. However, secondary displacements should accompany them. Strictly speaking, the observed displacements are the average of all the displacements caused by the inclusion of O3. When the accuracy of the measurement is improved, further displacements will be found and discussion of the anisotropic displacement parameters, including the anharmonic vibrations, will become important.

### 4.4. Comparison with theory and other experiments

The synchrotron X-ray diffraction at 90 K by Palacios *et al.* (2008) exhibited the shift of Al1. The O3 at the centre of the occupied cage is also displaced to a general position. The s.o.f.s of O3 at on- and off-centre sites are 0.106 (4) and 0018 (2). Lerch *et al.* (2009) concluded that O3 is located off-centre and also reported Al1a and a displaced Ca ion with elongated displacement ellipsoids along the  $\bar{4}$  axis. In the present study no O3 ions exist at the centre of the cage and further displacements of O1 and O2 ions were detected in our study.

The local structure obtained in the present study was compared with those obtained by theoretical calculations. Sushko *et al.* (2007) optimized the structure of the occupied cage in the process of energy minimization. They also reported the distortion of the occupied cage at Ca1<sup>0</sup>, Ca1<sup>iv</sup> and Al1<sup>iv</sup>, and the displacement of O3 to an off-centre site, in agreement with our result. However, most of the atomic distances in the occupied cage are different by more than ten times the experimental error. The distances Ca1b<sup>0</sup>–Ca1a<sup>iv</sup> and Al1a<sup>iv</sup>–O3<sup>iv</sup> in the present study are 4.481 (2) and 1.762 (9) Å compared with the theoretical values 4.39 and 1.88 Å. The distances between O3 and the Ca ions on the  $\bar{4}$  axis agree well

with our result. Although it was also reported that the difference of 0.3 Å in the bond lengths of  $\text{O3}^{\text{iv}}-\text{Al1a}^{\text{iv}}$  did not affect the electronic structure of the system, the theoretical calculation fixing the local structure of the occupied cage to that found in the present study is very interesting.

Theoretical studies on electrifieds derived from C12A7 (Sushko *et al.*, 2003*a,b*, 2007; Medvedeva & Freeman, 2004; Li *et al.*, 2004) presented different results in the localization of replaced electrons and the deformation of cages caused by them. Thus the change in displacement of the ions with the concentration of electrons, which are replaced with the O3 ions, is expected to present a stringent test for theoretical studies.

## 5. Conclusion

The crystal structure analysis revealed the displacements of all the ions around O3 except Al2 with the help of the electrostatic potential and electric field in the occupied cage. The refinement and assignment of constant s.o.f.s to all ions were successful, assuming a 1:1 ratio of displaced ions to O3, if the following holds:

(i) The inclusion of the  $\text{O3}^{\text{iv}}$  ion in a cage shifts  $\text{Al1}^{\text{iv}}$ , which is closest, by 0.946 (3) Å to  $\text{Al1a}^{\text{iv}}$ . As a result the  $\text{Al1}^{\text{iv}}-\text{O1}^{\text{ii}}$  bond is broken and a new  $\text{Al1a}^{\text{iv}}-\text{O3}^{\text{iv}}$  bond is formed.

(ii) The  $\text{Ca1}^{\text{0}}$  and  $\text{Ca1}^{\text{iv}}$  ions shift towards  $\text{O3}^{\text{iv}}$  by 0.810 (2) and 0.369 (2) Å to  $\text{Ca1b}^{\text{0}}$  and  $\text{Ca1a}^{\text{iv}}$ .

(iii) The electrostatic potential and electric field calculated in the present study worked well. The displacement of O1 and O2 by O3 was found in the occupied cage and the displaced oxygen ions which form a  $\text{AlO}_4$  tetrahedron with  $\text{Al1a}^{\text{iv}}$  were specified, except that of  $\text{O1}^{\text{iii}}$ .  $\text{O1}^{\text{iii}}$  may not be displaced or may be displaced to  $\text{O1b}^{\text{iii}}$  or there may be a third displacement of O1.

(iv) The third displacement of Ca1 to Ca1c is found and attributed to the loss of Al1 due to its shift to Al1a.

(v) The shape of the  $\text{Al1a}^{\text{iv}}$  tetrahedron is deformed significantly, in which very short  $\text{Al1a}^{\text{iv}}-\text{O1a}^{\text{i}}$  and  $\text{Al1a}^{\text{iv}}-\text{O2a}^{\text{iv}}$  bonds with lengths 1.431 (5) and 1.551 (8) Å coexist. The bond lengths of  $\text{Al1a}^{\text{iv}}$  to  $\text{O3}^{\text{iv}}$  and  $\text{O1b}^{\text{iii}}$  are 1.762 (9) and 2.051 (7) Å, although the displaced  $\text{O1}^{\text{iii}}$  ion is not completely determined. The bond length  $\text{Al1a}^{\text{iv}}-\text{O3}^{\text{iv}}$  reported by Palacios *et al.* (2008) was 1.73 Å.

(vi) The refinement was successful as a whole, since the minimum and maximum heights of the peaks on the final residual density are  $-0.39$  and  $0.37 \text{ e \AA}^{-3}$  and the *R* factor was reduced to 0.0161.

The present study revealed new displaced ions not found in previous studies and detailed local structure. We have presented a starting point for further studies on the electron density distribution of clathrated electrons in the electrified, C12A7:e. However, since the s.o.f. of O3 in the present crystal with no centre of symmetry is 1/24, extremely careful structure analysis of the non-centrosymmetric crystal as well as accurate intensity measurement was required and problems still remain. More accurate single-crystal diffraction experiments with higher accuracy and resolution, especially single-crystal

neutron diffraction experiments with high resolution, are needed.

We thank Professor N. Ishizawa and Dr J. Hester for providing instructions on data collection using PF-BL14A. TS also thank Dr R. Makita, Dr S. Funahashi, Mr T. Komori, Mr K. Okada and Dr I. Kagomiya for their kind advice.

## References

- Bartl, H. & Sheller, T. (1970). *Neues Jahrb. Miner. Monatsh.* **35**, 547–552.
- Boysen, H., Lerch, M., Stys, A. & Senyshyn, A. (2007). *Acta Cryst.* **B63**, 675–682.
- Bussem, W. & Eitel, A. (1936). *Z. Kristallogr.* **95**, 175–188.
- Chantler, C. T. (1995). *J. Phys. Chem. Ref. Data*, **24**, 71–643.
- Chantler, C. T. (2000). *J. Phys. Chem. Ref. Data* **29**, 597–1048.
- Christensen, A. N. (1987). *Acta Chem. Scand. A*, **41**, 110–112.
- Clementi, E. & Roetti, C. (1974). *At. Data Nucl. Data Tables*, **14**, 177–478.
- Coppens, P., Guru Row, T. N., Leung, P., Stevens, E. D., Becker, P. J. & Yang, Y. W. (1979). *Acta Cryst.* **A35**, 63–72.
- Hansen, N. K. & Coppens, P. (1978). *Acta Cryst.* **A34**, 909–921.
- Hayashi, K., Hirano, M. & Hosono, H. (2005). *Chem. Lett.* **34**, 586–587.
- Hayashi, K., Hirano, M., Matsuishi, S. & Hosono, H. (2002). *J. Am. Chem. Soc.* **124**, 738–739.
- Hayashi, K., Matsuishi, S., Kamiya, T., Hirano, M. & Hosono, H. (2002). *Nature*, **419**, 462–465.
- Hosono, H. & Abe, Y. (1987). *Inorg. Chem.* **26**, 1192–1195.
- Imlach, J. A., Glasser, L. S. D. & Glasser, P. F. (1971). *Cement Concrete Res.* **1**, 57–61.
- Jeevaratnam, F. P., Glasser, F. P. & Glasser, L. S. D. (1964). *J. Am. Ceram. Soc.* **47**, 105–106.
- Kim, S. W., Matsuishi, S., Nomura, T., Kubota, Y., Takata, M., Hayashi, K., Kamiya, T., Hirano, M. & Hosono, H. (2007). *Nano Lett.* **7**, 1138–1143.
- King, H. E. Jr & Finger, L. W. (1979). *J. Appl. Cryst.* **12**, 374–378.
- Kishimoto, S., Ishizawa, N. & Vaalsta, T. P. (1998). *Rev. Sci. Instrum.* **69**, 384–391.
- Kiyonagi, R., Richardson, J. W. Jr, Sakamoto, N. & Yoshimura, M. (2008). *Solid State Ionics*, **179**, 2365–2371.
- Lacerda, M., Irvine, J. T. S. & West, A. R. (1988). *Nature*, **332**, 525.
- Lerch, M., Janek, J., Becker, K. D., Berendts, S., Boysen, H., Bredow, T., Dronskowski, R., Ebbinghaus, S. G., Kilo, M., Lumey, M. W., Martin, M., Reimann, C., Schweda, E., Valov, I. & Wiemhöfer, H. D. (2009). *Prog. Solid State Chem.* **37**, 81–131.
- Li, J., Huang, F., Wang, Li., Yu, S. Q., Torimoto, Y., Sadakata, M. & Li, Q. X. (2005). *Chem. Mater.* **17**, 2771–2774.
- Li, Z., Yang, J., Hou, J. G. & Zhu, Q. (2004). *Angew. Chem. Int. Ed.* **43**, 6479–6482.
- Matsuishi, S., Hayashi, K., Hirano, M., Tanaka, I. & Hosono, H. (2004). *J. Phys. Chem. B*, **108**, 18557–18568.
- Matsuishi, S., Toda, Y., Miyakawa, M., Hayashi, K., Kamiya, T., Hirano, M., Tanaka, I. & Hosono, H. (2003). *Science*, **301**, 626–629.
- Medvedeva, J. E. & Freeman, A. J. (2004). *Appl. Phys. Lett.* **85**, 955–957.
- Miyakawa, M., Kim, S. W., Hirano, M., Kohama, Y., Kawaji, H., Atake, T., Ikegami, H., Kono, K. & Hosono, H. J. (2007). *J. Am. Chem. Soc.* **129**, 7270–7271.
- Palacios, L., Cabeza, A., Bruque, S., Garcia-Granda, S. & Aranda, M. A. G. (2008). *Inorg. Chem.* **47**, 2661–2667.

- Palacios, L., De La Torre, A. G., Bruque, S., Garcia-Muñ, J. L., Garcia-Garanda, S., Sheptyakov, D. & Aranda, M. A. G. (2007). *Inorg. Chem.* **46**, 4167–4176.
- Sakakura, T. (2008). *Software for Crystallography*. Personal communication.
- Sakurai, T. & Kobayashi, K. (1979). *Rep. Inst. Phys. Chem. Res.* **55**, 69–77.
- Satow, Y. & Iitaka, Y. (1989). *Sci. Instrum.* **60**, 2390–2393.
- Shannon, R. D. & Prewitt, C. T. (1969). *Acta Cryst.* **B25**, 925–946.
- Sushko, P. V., Shluger, A. L., Hayashi, K., Hirano, M. & Hosono, H. (2003a). *Phys. Rev. Lett.* **91**, 26401.
- Sushko, P. V., Shluger, A. L., Hayashi, K., Hirano, M. & Hosono, H. (2003b). *Thin Solid Films*, **445**, 161–167.
- Sushko, P. V., Shluger, A. L., Hayashi, K., Hirano, M. & Hosono, H. (2007). *J. Am. Chem. Soc.* **129**, 942–951.
- Takenaka, Y., Sakakura, T., Tanaka, K. & Kishimoto, S. (2008). *Acta Cryst.* **A64**, C566.
- Tanaka, K., Kumazawa, S., Tsubokawa, M., Maruno, S. & Shirotani, I. (1994). *Acta Cryst.* **A50**, 246–252.
- Tanaka, K. & Saito, Y. (1975). *Acta Cryst.* **A31**, 841–845.
- Vaalsta, T. P. & Hester, J. R. (1997). *Diff14A* Software. Photon Factory, Tsukuba, Japan.